Available online at www.sciencedirect.com
ScienceDirect
Current Opinion in Solid State and Materials Science 11 (2007) 3–18
Current Opinion in Solid State & Materials Science

TiO_2 nanotubes: Self-organized electrochemical formation, properties and applications

J.M. Macak, H. Tsuchiya [1], A. Ghicov, K. Yasuda [2], R. Hahn, S. Bauer, P. Schmuki *

Department of Materials Science, LKO, University of Erlangen – Nuremberg, Martensstr. 7, 91058 Erlangen, Germany

Received 28 August 2007; accepted 30 August 2007

Abstract

The present paper gives an overview and review on self-organized TiO_2 nanotube layers and other transition metal oxide tubular structures grown by controlled anodic oxidation of a metal substrate. We describe mechanistic aspects of the tube growth and discuss the electrochemical conditions that need to be fulfilled in order to synthesize these layers. Key properties of these highly ordered, high aspect ratio tubular layers are discussed. In the past few years, a wide range of functional applications of the layers have been explored ranging from photocatalysis, solar energy conversion, electrochromic effects over using the material as a template or catalyst support to applications in the biomedical field. A comprehensive view on state of the art is provided.

Keywords: Self-organization; Titanium dioxide; Electrochemical anodization; Nanotubes

1. Introduction

1.1. General

The successful synthesis of carbon nanotubes by Iijima in 1991 [1] stimulated intense research activities world-wide due to the anticipated technological impact of this unique combination of material, directionality and enhanced properties, such as quantum size effects. In the following years the successful chemical (hydrothermal) synthesis of various other nanotubes, in particular transition metal oxide nanotubes – such as TiO_2 or V_2O_5 was reported [2–4]. In order to exploit nanotubes in many devices, it is essential to orient nanotubes on substrates and to create ordered arrays. Many different approaches have been explored that mainly are based on lithography, using nano-tools (e-beam, X-ray, ion beam, STM, AFM), or, more elegantly, rely on self-alignment processes.

Among the simplest, cheapest and most straight-forward approaches that lead to ordered nanostructures are anodization techniques that can – under the 'right' conditions – lead to highly ordered porous systems (see Fig. 1a). The best explored case is Al and the growth of self-ordered porous alumina layers [5–14]. For Al, it has been known for decades [5,6] that porous oxide layers can be grown by anodization typically in acidic electrolytes, while anodization in neutral electrolytes typically leads to a compact oxide layer. However it was not until the remarkable work of Masuda et al. [9] that it became clear that a very high degree of order can be achieved for these porous geometries. Ordered alumina structures have been proposed, for example, to be used as a photonic crystal structures [14], or as a template for the deposition of other materials [15–17].

More recently, for a range of other metals such as Ti [18–43], Zr [44–47], Nb [48–52], W [53–55], Ta [56–58], Hf [59] it has been found that self-organized porous structures can be formed under optimized electrochemical treatments.

* Corresponding author.
E-mail address: schmuki@ww.uni-erlangen.de (P. Schmuki).
[1] Present address: Division of Materials and Manufacturing Science, Graduate School of Engineering, Osaka University, 2-1 Yamada-oka, Suita, Osaka 565-0871, Japan.
[2] Present address: Institute of Industrial Science, The University of Tokyo, 4-6-1 Komaba, Meguro-ku, Tokyo 153-8505, Japan.

1359-0286/$ - see front matter © 2007 Elsevier Ltd. All rights reserved.
doi:10.1016/j.cossms.2007.08.004

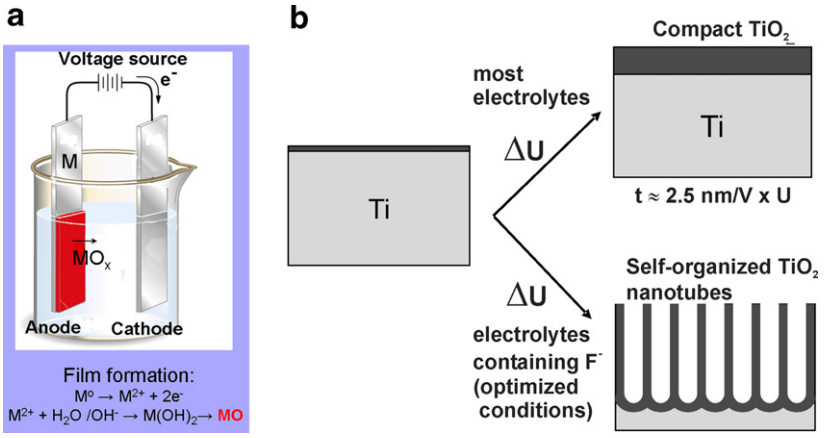

Fig. 1. Schematic set-up for anodization experiments. Anodization leads to an oxidation of metal species that form a solid oxide on the metal surface (a). Depending on the anodization conditions (mainly potential, electrolyte, temperature), the solid oxide layer can be either compact, or nanotubular (nanoporous). To achieve an ideal self-ordering of the nanotubes, use of the optimized anodization parameters is crucial.

1.2. TiO_2

Particularly the case of TiO_2 stimulated significant research activity as TiO_2 is a material with a number of almost unique properties used for many years in various functional applications – an overview is shown in Table 1. For Ti and other so-called valve metals it has been known for more than 50 years that it is possible to grow compact oxide layers of considerable thickness (some 100 nm) by anodization in aqueous electrolytes [60,61]. Typically growth occurs proportional to the applied potential with a growth factor $f_g \approx 1$–5 nm/V [62] up to a voltage, where dielectric breakdown of the oxide occurs [63,64]. The structure of the as grown oxide can be amorphous or crystalline, strongly dependent on the specific electrochemical parameters such as the applied potential, the time of anodization, or the sweep rate of the potential ramp. For example, the structure of the oxide films on Ti has typically been reported to be amorphous at low voltages (below 20 V [65]), and crystallization to take place at higher voltages. Depending on the anodizing conditions the crystal structure has been reported to be anatase [63–67], a mixture of anatase and rutile [63,67,68], or rutile [63,67].

A completely different growth morphology can be obtained, if fluoride ions are present in electrolytes and suitable anodization conditions are used. Ordered nanotubular/nanoporous structures of TiO_2 or other transition metal oxides can be formed as schematically shown in Fig. 1b. In general, the morphology and the structure of porous layers are affected strongly by the electrochemical conditions (particularly the anodization voltage) and the solution parameters (in particular the HF concentration, the pH and the water content in the electrolyte).

The first generation of the TiO_2 nanotube arrays was grown in HF electrolytes or acidic HF mixtures [18–20]; an example of the typical morphology is shown in Fig. 2A. These layers showed a limited thickness that would not exceed 500–600 nm. By using buffered neutral electrolytes containing NaF or NH_4F instead of HF [21–24] and taking into account the importance of the pH gradient within the tube [22], it was shown that self-organized nanotube TiO_2 layers with thicknesses higher than 2 μm could be grown [21–24]. The third generation nanotubes were grown in (almost) water free electrolytes. Earlier work carried out in glycerol electrolytes (see Fig. 2B) showed tubes with extremely smooth walls and a tube length exceeding 7 μm [25], while using CH_3COOH electrolytes [26] remarkably small tube diameters could be obtained. Meanwhile, for example in aged ethylene glycol electrolytes and by a further optimization of parameters, the nanotube length has reached 260 μm [29] and the tubes have an almost ideal hexagonal arrangement [69], an example is shown in Fig. 2C.

Table 1
TiO_2 applications

TiO_2 application	Reference
Photocatalysis	[135,128,129,181]
Self-cleaning, wetting	[152,153]
Solar cell	[126,127]
Catalysis	[182,183]
Gas sensing	[184,185]
Doping	[105,108]
Biomedical	[157,161]
Ceramics	[186,187]
Interference coating, optical devices	[188,189]

1.3. Other transition metals

In parallel to activities on TiO_2, this surprisingly simple nanostructuring approach was implemented also for many other valve metals such as Zr [44–47], Nb [48–52], W [53–55], Ta [56,57] and Hf [59]. In all these works, fluoride anion containing electrolytes were used as an electrolyte for a controlled anodization of metals under anodic bias applied for several hours and leading to the growth of self-organized oxide layers on their surfaces. In contrast

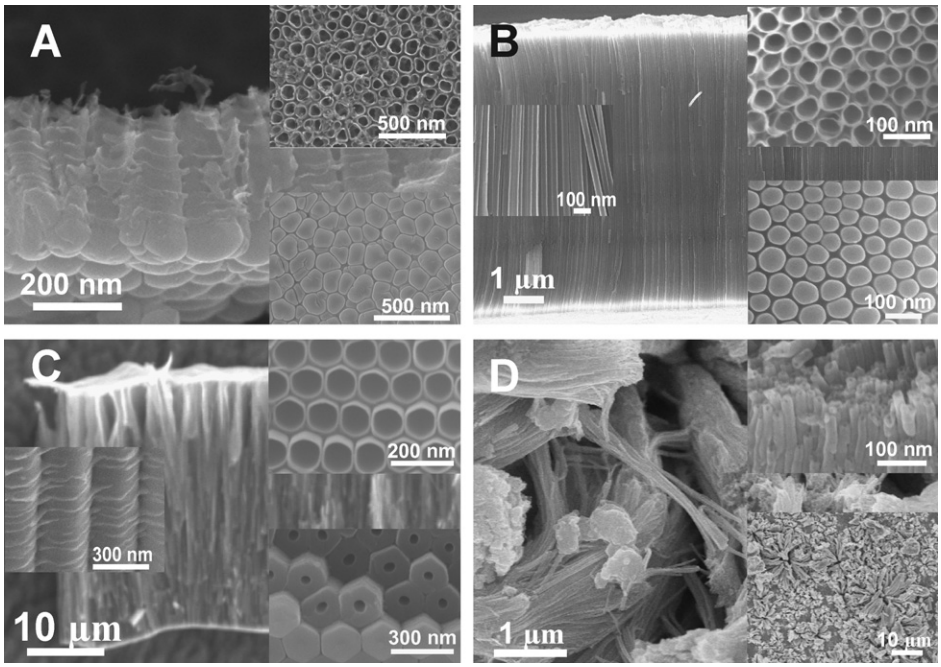

Fig. 2. SEM images showing TiO_2 nanotube layers grown by different anodization processes of Ti. (A) Typical morphology obtained in acidic fluoride or HF electrolytes, (B) glycerol/fluoride electrolytes, (C) ethylene glycol/fluoride electrolytes. The insets show top-views (open tubes), bottom views (closed ends) and side walls in detail. (D) tubes grown by a different approach: rapid breakdown anodization (RBA); these tubes grow in disordered bundles within seconds at comparably high anodic potentials. The upper inset in (D) shows a side view of the layer, the lower inset shows a low magnification of the surface.

to alumina, anodization of Ti, Hf and Zr leads to formation of metal oxide nanotubes (hollow cylinders) perpendicular to the substrate and separated from each other by a gap. In the other cases (W, Nb, Ta), anodization leads to the growth of porous oxide layers.

1.4. Alloys

Particularly interesting is the growth of nanotubes on various alloys, as this increases drastically the potential functionality of the tubes (by e.g. incorporation of doping species in the oxide structure). Also it shows that nanotube layers can be applied as surface coatings on various technical alloys. Using the same approach as for Ti, that is, controlled anodization in dilute fluoride electrolytes, recently on intermetallic compounds such as TiAl [70], binary alloys such as TiNb [71], TiZr [72,73], or on complex biomedical alloys such as Ti6Al7Nb [74] and Ti29Nb13Ta4.6Zr [75,76] nanotube layers have successfully been grown. Examples are shown in Fig. 3 for Ti6Al7Nb (A), TiAl (B), TiNb (C), and TiZr (D).

For TiNb, surprising synergistic effects on the growth morphologies of the oxide nanotubes were found [71]. It was shown that the range of achievable diameters and lengths of TiO_2-based nanotubes can be significantly expanded, if a binary Ti–Nb alloy, rather than pure Ti, is used as a substrate. The length of the resulting mixed oxide nanotubes can be adjusted from 0.5 to 8 μm, and the diameter from 30 to 120 nm. The morphology of the tubes differs significantly from that of the nanostructures grown under the same conditions on pure Ti or Nb substrates: only considerably shorter tubes grow on Ti, whereas irregular porous structures grow on Nb.

For anodic nanotubes formed on TiZr alloys [33,72,73] the morphological character of the oxide nanotubes is between those of titanium oxide and zirconium oxide nanotubes. The nanotubes have a straight and smooth morphology with a diameter ranging from 15 to 470 nm and a length up to 21 μm depending on the terminal anodization potential (i.e. they show a largely expanded structural flexibility compared with nanotubes formed on the individual elements).

The alloy Ti29Nb13Ta4.6Zr has been developed by Niinomi et al. for biomedical applications, in order to reduce the elastic modulus of titanium alloys to the level of living bone [77]. Self-organized oxide nanotubes grown on this alloy [75,76], except for a high degree of structural flexibility, can show a very spectacular feature that is multiscale self-organization, (oxide nanotube arrays with two discrete sizes and geometries). This feature recently has been investigated in more detail using TiZrNb [78] and TiNb alloys [79] showing that even for binary alloys two size scale self-organization (as in Fig. 7) can be obtained.

Attempts have been made to grow self-organized anodic tube layers on technologically relevant substrates such as Ti6Al4V and Ti6Al7Nb [18,74]. However, these approaches suffered typically from two problems: (1) the selective dissolution of less stable elements, and (2) the different reaction rates on different phases of an alloy. Therefore "ideal" alloys for nanotube formation possess

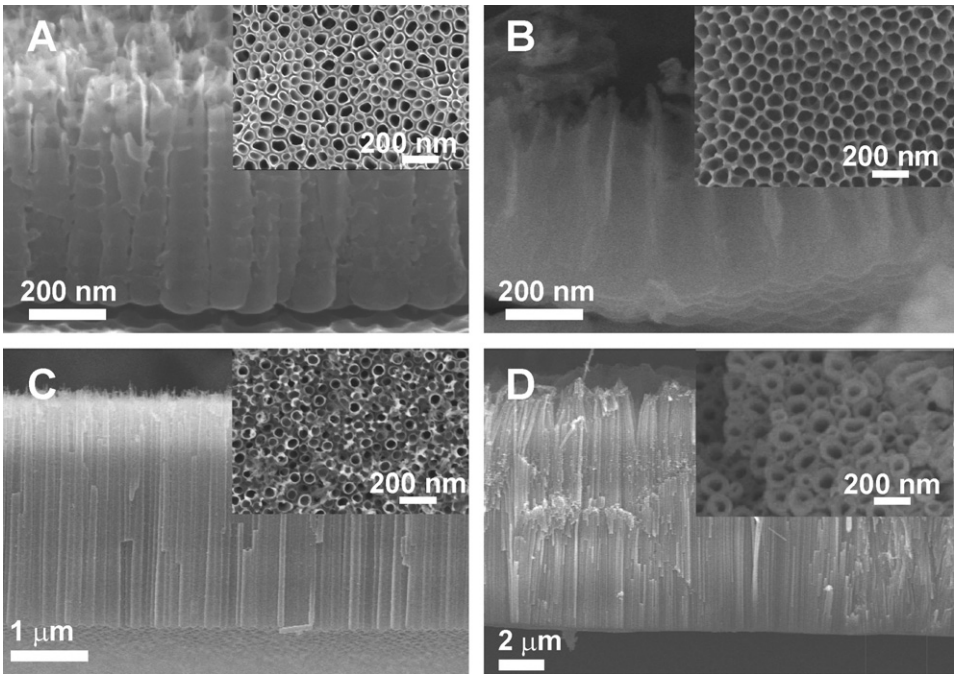

Fig. 3. SEM images showing self-organized oxide nanotube layers grown on Ti6Al7Nb alloy (A), TiAl intermetalic compound (B), TiNb alloy (C) and TiZr alloy (D) by anodization in fluoride containing $(NH_4)_2SO_4$ electrolytes. The insets show top-views of the nanotube layers.

a single-phase microstructure and a composition that essentially only contains valve metals. Additionally one may note that recently it was demonstrated that also for the Al case, neutral F-containing solutions can be used to achieve fast and highly ordered oxide structures [80].

1.5. RBA tubes

It should be mentioned that also fundamentally different approach for the growth of anodic TiO_2 nanotubes has recently been reported. This so-called RBA (rapid breakdown anodization) approach leads to bundles of nanotubes, as shown in Fig. 2D, that grow within tens of seconds typically in perchlorate or chloride containing electrolytes at considerably high voltages (sufficiently high to create a local breakdown of the oxide film that then represents the nucleus for the tube-bundle growth). Based on an original report of Nakayama et al. [81] it was shown that the principle can be used in chloride or perchlorate solutions [82,83] and also be applied to other materials [82]. While being fast, the approach seems not easily to be tunable to become self-organized and will therefore not extensively be considered in this review.

Overall, self-organized nanotubes made of TiO_2 combine geometrical advantages given by their array structure with the material specific properties of TiO_2. As mentioned above, TiO_2 is used in many functional applications (examples are listed in Table 1). Many of these applications are based on the specific semiconducting properties of TiO_2 (particularly anatase) that is a wide band gap n-type semiconductor, with a sufficiently low (anodic) valence band edge to allow a photo-induced generation of highly reactive $OH^{\cdot}$ radicals. Strategies to exploit TiO_2 nanotubes for applications usually try to combine a specific feature of TiO_2 with the tubular geometry – such approaches will be outlined later in this review.

2. Formation and growth

2.1. Stages of growth

The anodic growth of compact oxides on metal surfaces and the formation of tubes are, in the most simple approach, governed by a competition between anodic oxide formation according to reaction (1)

$$Me + 2H_2O \rightarrow MeO_2 + 4H^+ + 4e^- \quad (1)$$

and chemical dissolution of the oxide as soluble fluoride complexes, e.g.;

$$MeO_2 + 6F^- \rightarrow [MeF_6]^{2-} \quad (2)$$

Respectively direct complexation of high-field transported cations at the oxide electrolyte interface:

$$Me^{4+} + 6F^- \rightarrow [MeF_6]^{2-} \quad (3)$$

Reaction (1) describes the oxide growth on an anodized metal surface, as schematically depicted in Fig. 4a in a fluoride-free electrolyte. Oxidized metal species react with O^{2-} ions (from H_2O) to form an oxide layer. Further oxide growth is controlled by field-aided ion transport (O^{2-} and Ti^{4+} ions) through the growing oxide. As the system is under a constant applied voltage, the field within the oxide is progressively reduced by the increasing oxide thickness, the process is self-limiting. Fig. 5a shows a

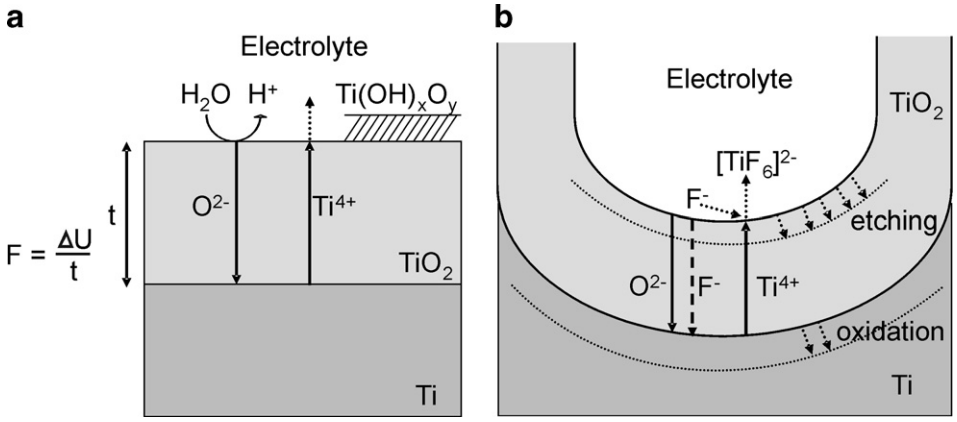

Fig. 4. Schematic representation of the Ti anodization (a) in absence of fluorides (results in flat layers), and (b) in presence of fluorides (results in the tube growth).

schematic current–time transient for anodization of Ti in a fluoride-free electrolyte (e.g. H_2SO_4). The decreasing field strength leads to an exponential current decay and thus to the growth of a compact oxide layer with a finite thickness. If Ti^{4+} ions arriving at the oxide/electrolyte interface are not 'made soluble' by complexation, a hydroxide layer will precipitate in most electrolytes [23]. This layer typically is loose and porous and thus does not contribute to field effects, but exerts to a certain extent diffusion retarding effects.

In the presence of fluoride ions the situation becomes less straight-forward as shown schematically in Fig. 4b. This is mainly due to two effects of the fluoride ion: (i) the ability to form water-soluble TiF_6^{2-} complexes according to reaction (2), and (ii) the small ionic radius that makes them suitable to enter the growing TiO_2 lattice and to be transported through the oxide by the applied field (thus competing with O^{2-} transport). The complex formation ability leads to a permanent chemical attack (dissolution) of formed TiO_2 and prevents $Ti(OH)_xO_y$ precipitation as Ti^{4+} ions arriving at the oxide/solution interface can be solvatized to TiF_6^{2-} (reaction (3)), before reacting to a precipitate $Ti(OH)_xO_y$ layer. As a result, the current–time curve for electrolyte containing fluorides deviates from the classical high-field growth (Fig. 5a). That is, after an initial exponential decay (phase I) the current increases again (phase II) with a time lag that is shorter, the higher the fluoride concentration. Then, the current reaches a quasi-steady state (phase III). This steady state current increases with increasing fluoride concentration [20].

This type of current–time curve has been previously reported for self-organized pore formation for other materials, as well [84]. Typically, such a current behavior can be ascribed to different stages in the pore formation process, as schematically illustrated in Fig. 5b. In the first stage, a barrier oxide is formed, leading to a current decay (I). In the next stage, the surface is locally activated and pores start to grow randomly (II). Due to the pore growth the active area increases and the current increases. After some time, many pores have initiated and a tree-like growth takes place. Therefore, the individual pores start interfering with each other, and start competing for the available current. This leads under optimized conditions to a situation where the pores equally share the available current, and self-ordering under steady state conditions is established (III). Indeed, if the pore initiation phase is followed in a concrete case by SEM images, exactly the sequence described in Fig. 5b can be observed [23].

The fact that the layer thickness and the current density reach a limiting value after a certain polarization time can be explained by a steady state situation depicted in Fig. 5c. During anodization continual growth of oxide takes place at the inner interface, and chemical dissolution of the oxide layer occurs simultaneously. Steady state is established when the pore growth rate at the metal oxide interface is identical to the thickness reducing dissolution rate of the oxide film at the outer interface. In this situation the nanotube oxide layer just continuously "eats" through the titanium substrate without thickening of the oxide layer. As the steady state current densities are typically considerably high, this occurs even with comparably high velocity. This finding also explains the typically low current efficiencies (for oxide formation) in acidic electrolytes (3–10%), and in particular their continuous drop with extended anodization time.

It should be remarked that the chemical dissolution of TiO_2 occurs of course over the entire tube length, thus the tubes with extended time become increasingly v-shaped in morphology, i.e., at the tops the tubes possess significantly thinner walls than at their bottoms [33,73]. The reason for separation into tubes, as opposed to a nanoporous structure, is not yet entirely clear, however, it may be ascribed to accumulation of fluoride species at the tube bottom and thus to establishment of an anion containing weaker (and more soluble) TiO_2 structure between neighboring pores/tubes.

Regarding the growth velocity of the tubes and the rate-determining step, it is clear that a longer growth times (after generally several minutes), growth becomes diffusion

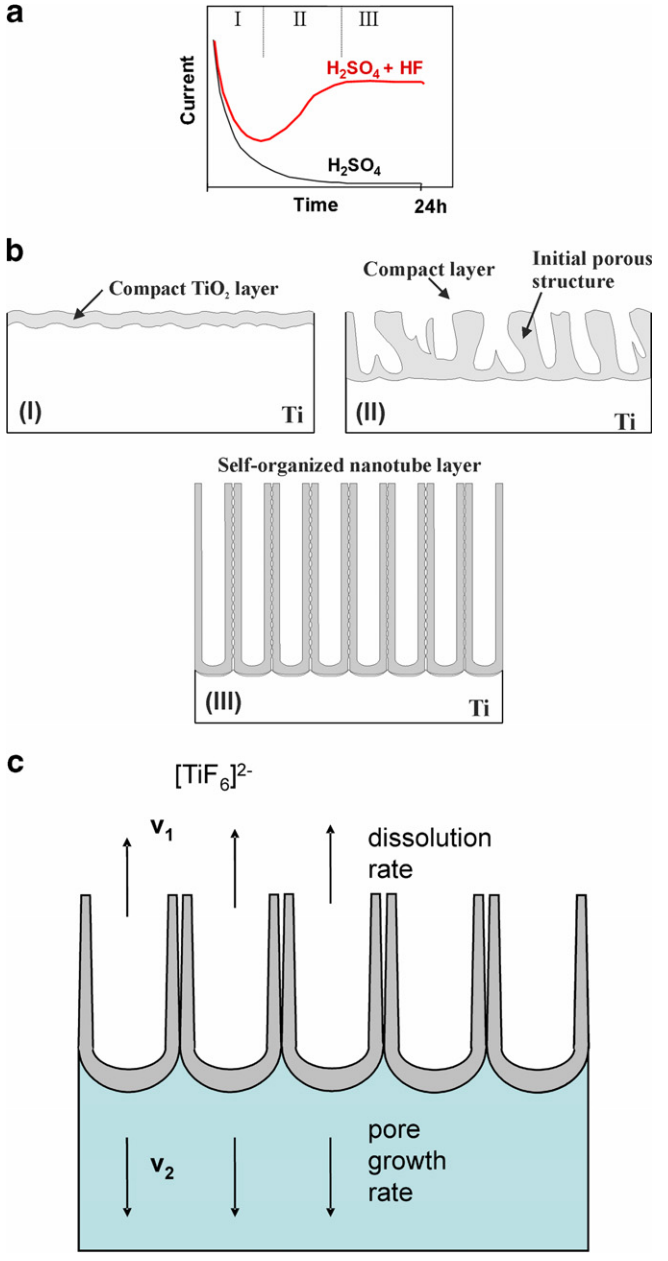

Fig. 5. (a) Characteristic current transients for Ti anodization with and without fluorides in the electrolyte; (b) corresponding evolution of the TiO_2 morphology; (c) steady state growth situation characterized by equal rates of TiO_2 dissolution (v_1) and formation (v_2).

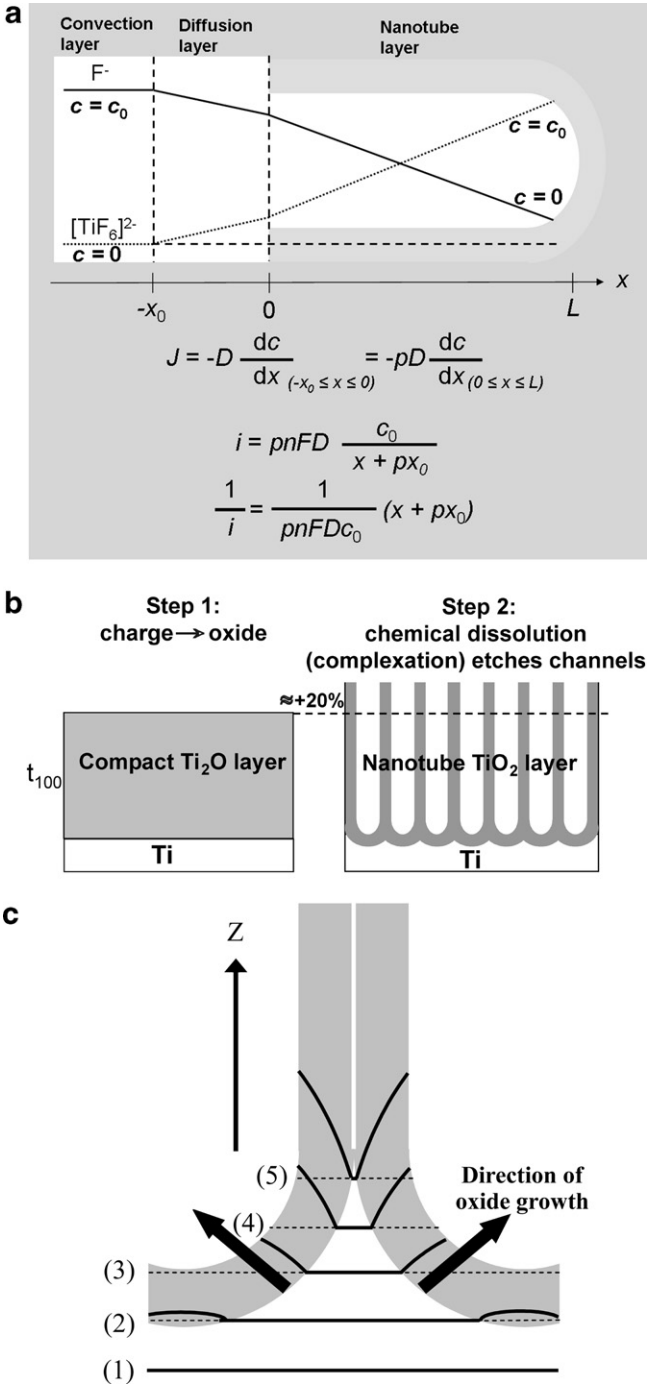

Fig. 6. (a) Model for diffusion controlled growth of tubes: assumed is diffusion of TiF_6^{2-} within tube with porosity p and adjacent diffusion layer in electrolyte controls anodic current. This leads to a straight relationship $1/i \sim t$; (b) model for evaluating current efficiency: assuming that all the charge is converting Ti to TiO_2, a theoretical thickness t_{100} is obtained. This approximately is observed in experiments. However, detailed analysis shows that typically even a length expansion in the order of 20% is obtained. This can be explained by (c); (c) model for length expansion, Stress 'pushes' some of the oxide up the wall, flow of oxide species in direction of the tube wall takes place [33,73].

controlled as schematically depicted in Fig. 6a. This means that the diffusion of fluoride species to the tube bottom, or the transport of reacted TiF_6^{2-} species becomes current determining. Up to the moment, when chemical dissolution of the tubes starts significantly shortening the tubes, also the length of the tubes is therefore diffusion controlled [73]. The model outlined in Fig. 6 that $1/i$ is proportional to the tube length is indeed observed for many systems [73]. Considering the connection between the tube length and the total electrical charge, an appropriate model is to assume that first all the current (charge) results in an oxide of a given thickness, then dissolution (and complexation) just chemically etches channels in this material. In other words, the thickness of the tube layer is essentially reflected by the thickness of a hypothetical, corresponding compact

layer. This means that in terms of tube length, a 100% current efficiency would be obtained, while in terms of oxidized mass (or volume) due to the channels, of course, a lower efficiency is obtained. In general, this model holds well in the early stages of the tube growth [73], however, surprisingly one finds in experiments that tubes are even ≈10–20% longer than this 100% length efficiency expectation (as depicted in Fig. 6b) – thus it has been proposed that during tube growth a flow mechanism is operative [33] as observed for Al [190] that pushes the oxide up the wall as schematically shown in Fig. 6c (for example due to stress effects) and therefore leads to the a priori surprising length expansion.

2.2. Effect of anodization voltage

The key factor controlling the tube diameter is the anodization voltage [31,86]. Fig. 7 shows a diameter dependence on the potential for the TiO_2, ZrO_2 and Nb_2O_5 nanotube layers. Particularly in the case of TiO_2 nanotubes layers, a wide variety of nanotube diameters can be achieved. For anodization experiments carried out in 1 M $H_3PO_4 + 0.3$ wt% HF it has been shown that the tube diameter can be grown in the range of 15–120 nm in the potential range between 1 and 25 V [31]. Particularly remarkable is that self-organized structures are obtained even at potentials as low as 1 V, although the morphology shows rather a web like structure rather than a clear tubular morphology. Recently, for mixed glycerol–water electrolytes containing 0.27 M NH_4F, the tube diameter range was further extended from 20 up to 300 nm in the potential range between 2 and 40 V [86]. At potentials higher than 40 V, however, the formed layers were no longer self-organized. This level of diameter control bears significant potential for applications where the tube diameter needs to be tailored for specific use, such as e.g. when a defined size for embedding of biological species is desired.

In non-aqueous electrolytes, typically higher voltages are reported to grow tubes of a given diameter. At present, these higher values must, however, be attributed to the typically very significant IR drop that occurs in these electrolytes. It appears, that in general the tube diameter can be described by $d = k \times V$, where k is essentially equal to $2f_g$ (f_g being the growth factor for anodic oxides, ≈2.5 nm/V for TiO_2). Similar finding holds also for Zr and Nb, although the diameter increase with increased applied potential is not so steep [44–46,71].

Fig. 7b gives an overview of the diameter dependence for some alloys that show self-organization on two size scales. An example of a bottom view of a two size scale nanotube layer is given in Fig. 7c. In this case, the large diameter (200 nm for TiZr and 300 for TiNb) typically corresponds to f_g of Ti, while the smaller diameter is likely due to the geometrical situation. In other words, the smaller diameter tube grows recessed [75,78,79] and thus has less anodizable metal area available as schematically shown in the inset of Fig. 7c.

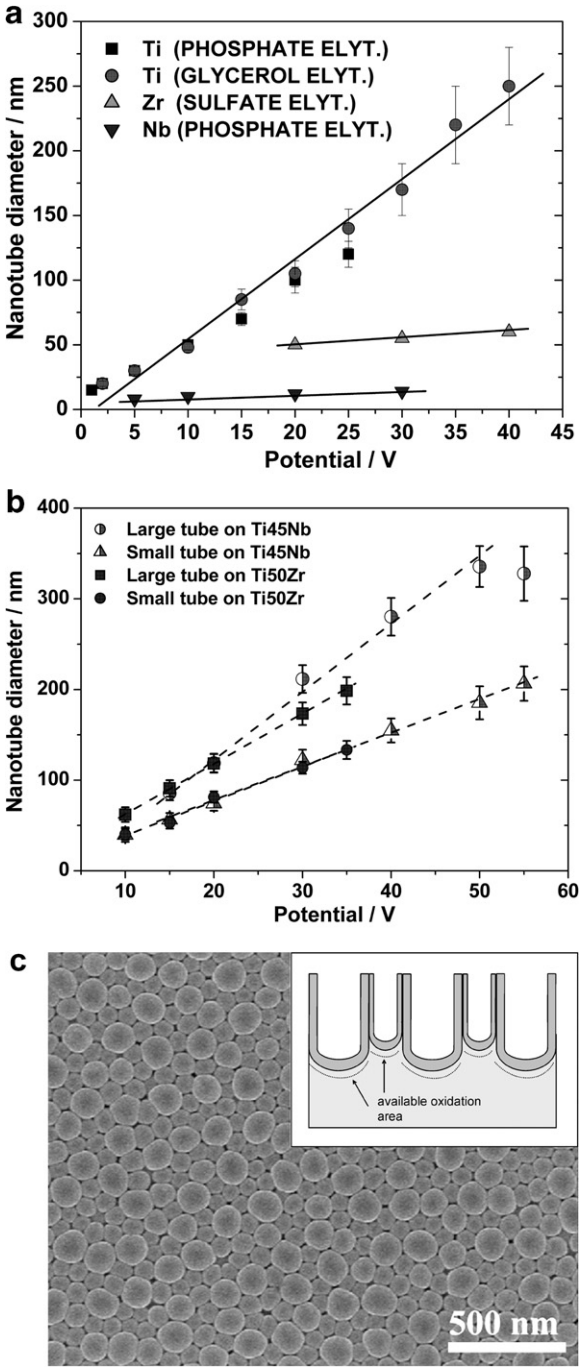

Fig. 7. Tube diameter as a function of the applied potential for self-organized nanotubes on (a) Ti in different electrolytes, and (b) for TiNb and TiZr alloys; (c) SEM image of TiNb nanotube layer showing two size self-organization of the diameter with an inset that shows schematically the origin of two size scale tubes due to the recession of smaller diameter tubes.

2.3. Ideal ordering

Recently, it has been shown that the tubes grown in ethylene glycol electrolytes show a hexagonal close-packed

structure [69] (as apparent e.g. from the tube bottom, compare insets in Fig. 2C), i.e. essentially the same arrangement as it is observed in so-called porous anodic alumina layers [9,10]. Several factors strongly influence the degree of ordering [69]: (i) the anodization voltage (apparently the highest possible voltage just below dielectric breakdown seems most appropriate), (ii) the purity of the material (certain ordering faults can be eliminated by using a high purity Ti). Furthermore, repeated anodization, as in the case of Al, can clearly improve the ordering. By using this approach, the bottom imprints of a first tube layer in the underneath Ti act as "pre-ordering" guides for a subsequent anodic tube initiation and growth.

2.4. Current oscillations

It has been reported that periodical current oscillations can occur during the anodization process that can be very regular and can be maintained for more than 24 h [20,25]. The origin of these oscillations is not understood in detail, but it is interesting that the periodicity of the oscillations can be correlated with the regularly spaced ripples at the sidewalls of the tubes, for example apparent in Fig. 2A.

2.5. Different morphologies, such as multilayers and free-standing membranes

By changing the electrochemical conditions during the anodization process, for a range of valve metal oxides, multilayered structures can be grown [85,87]. An example is shown in Fig. 8a. In other words, first a layer under a first parameter set may lead to a first geometry, then underneath a second layer of tubes can be grown with a different parameter set. Interestingly, the underneath layer may be initiated at the bottom of a tube (to break through the bottom of a tube) [87], or in the spaces between the tubes [85]. Such multilayer stacks may have a variety of applications, wherever critical tailoring of properties is needed.

Even more spectacular is the formation of free-standing, both-side open membranes [88] as a whole range of functionalization may be accessed including for example flow-through photoreactors. An example of the nanotube membrane is shown in Fig. 8b.

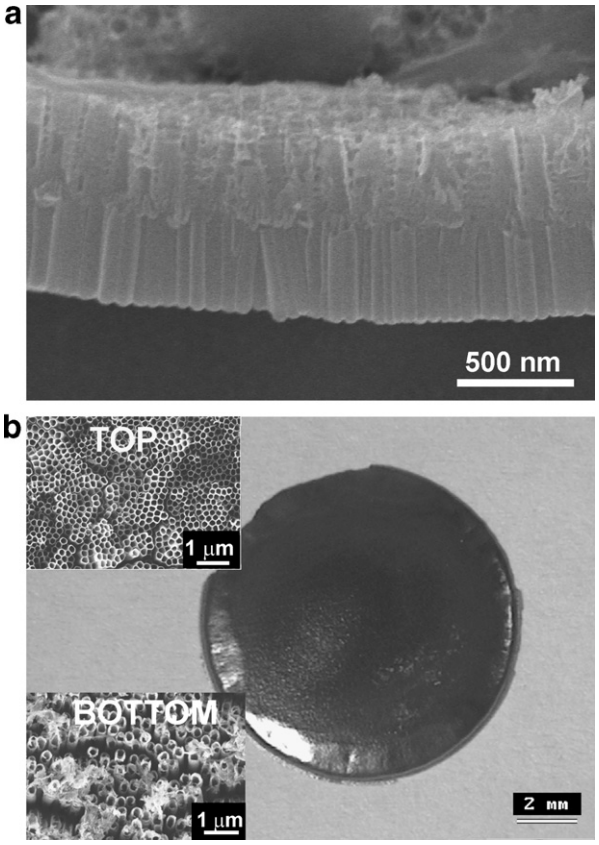

Fig. 8. (a) TiO_2 nanotube double layer stack produced by repeated anodization under different conditions (upper layer has a diameter of 100 nm, lower layer of 40 nm); (b) optical image of free-standing TiO_2 nanotubular membrane of 140 μm thickness and 1 cm diameter, open on both-sides; the insets show top and bottom SEM images.

3. Properties of the tubes

3.1. Structure, annealing, chemistry

3.1.1. Crystallographic structure

As-formed TiO_2 tubes typically have an amorphous structure. Several studies show that the tubes can be converted to anatase at temperatures higher than approximately 280 °C in air [89–92] or a mixture of anatase and rutile at temperatures higher than approximately 450 °C [89,90]. Most recently, there are indications that already in the as-formed tubes under certain conditions nano-crystallites can be present [86,93].

Fig. 9a shows a comparison of XRD patterns of nanotube samples after their formation (amorphous), after annealing at 450 °C (anatase), and after annealing at 550 °C (mixture of anatase and rutile). Fig. 9b shows high-resolution transmission electron microscope (HRTEM) images of the bottom of nanotubes before and after annealing at 450 °C, and selected area diffraction patters (SAED) of the tube bottoms taken from the corresponding images (as insets) that also confirm the conversion to anatase [91]. From XRD measurements one can obtain that the major anatase orientation is the (101) plane. Other planes, such as i.e. (200) and (105) are only present in a minor amount. For the nanotube layers typically crystal growth starts at the tube bottom via interface nucleation, due to the larger space available for crystal growth than in the side wall. For certain tubes it was found that essentially over the entire length only one plane – (101) – is present along the walls. This points to the possibility to grow single crystalline tubes [91,92].

Annealing under oxygen-free conditions (e.g. in argon atmosphere) leads to a blackening of the tube layers due to a significant reduction of the Ti(IV)-species in the oxide to Ti(III). Such structures typically have a very limited mechanical stability [90]. Introducing alloying elements

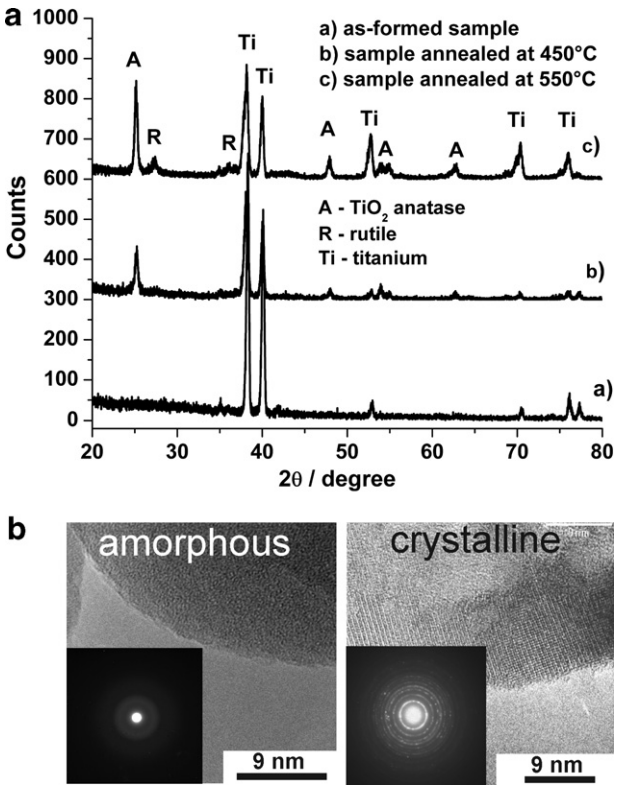

Fig. 9. (a) XRD of as-formed amorphous TiO_2 nanotube layer and crystalline layers annealed at 450 °C and 550 °C; (b) corresponding HRTEM images of the samples, insets show diffraction patterns (SAED) taken at the same locations. Annealing was performed for 3 h in air.

such as Nb [94] or C [95] into the TiO_2 significantly increases the temperature of the anatase-to-rutile conversion, and shifts also the temperature of structural collapse to a higher value. For TiNb, the oxide tubes consist of an amorphous mixed TiO_2–Nb_2O_5 structure [71]. After annealing at 450 °C, anatase-type TiO_2 appears in XRD. After annealing at 650 °C, an additional peak assigned to rutile appears, but the major TiO_2 phase remains anatase with a crystallite size of 25 nm. This result shows that the anatase–rutile transition takes place at a higher temperature in the polycrystalline mixed oxide nanotubes than in pure TiO_2. Weak reflections assigned to pseudo-hexagonal Ti–Nb_2O_5 can be detected after annealing at 650 °C. Apart from the retardation of the anatase–rutile transition by Nb_2O_5, it is also remarkable that the mixed oxide nanotubes are stable to annealing at 650 °C [71]. For pure TiO_2 nanotubes treated at this temperature, a substantial collapse of the tubular morphology has been reported [89].

In contrast to nanotubes formed on TiNb, the tubes grown on TiZr consist of a zirconium titanate oxide – as-formed, with an amorphous structure that can be crystallized after adequate heat treatment [72].

3.1.2. Chemical composition

As-formed tubes on Ti show in XPS and investigations a composition of TiO_2 with minor contents of hydroxides on the surface of the tube walls [23]. Different background ions in the electrolyte are integrated into the tube structure at different concentration levels. While ClO_4^- ions are hardly incorporated, SO_4^{2-} and particularly PO_4^{3-} are incorporated into the entire tube to significant levels (some few atomic %). Very clear is that significant amounts of F^- (≈1–5 at.%) are entering the TiO_2 structure. This is in line with some earlier work on the anodization of Ti in fluoride containing electrolytes [96]. Recent TEM investigations indicate that fluorides indeed are accumulated (before annealing) at the metal/oxide interface and to a certain extent between the individual tubes.

Annealing leads to almost complete loss of the fluorides at around 300 °C [91] and clearly the amount of surface hydroxides is reduced [32,97].

3.2. Semiconducting properties

Typically the semiconducting properties of the tubes were up to now characterized mainly for pure TiO_2 in terms of their photoresponse [90,98–101] and their capacitance behavior (Mott–Schottky plots) [100–102].

3.2.1. Photoresponse of the tubes

For TiO_2 nanotubes, typical photocurrent characteristics for the as-formed and annealed samples (at 450 °C) are provided in Fig. 10 as IPCE-plots [91,98,100]. The insets give the corresponding (IPCE $h\nu)^{1/2}$ vs. $h\nu$ plots to determine the indirect band gap of the material, it results for the annealed samples as 3.15 ± 0.05 eV, which is in line with typical value reported for anatase [103]. It is evident that the IPCE upon annealing is drastically increased. It has been deduced that for the as-formed tubes most of the photocurrent is generated in the bottom of the tubes [98] and the tube wall contribution is negligible (as the amorphous structure provides a high number of defects that lead to a high carrier recombination rate). The drastic increase of the photocurrent after annealing indicates that by a conversion to anatase the tube walls are activated and contribute to the photocurrent [98]. The plot in Fig. 10b shows also the strong effect that the tube length has on the overall photoresponse [104]. Clearly the photoresponse is dominated by two controversial factors: (i) the longer the tubes, the higher the total light absorption, and (ii) the longer the tubes, the higher the recombination losses (for electrons photo-generated in the outermost part of the nanotube structure). Experimentally, the optimum tube length (for UV conversion) is around 1 μm (depending, of course, on the wavelength) [104]. However, further investigations of the photoelectrochemical response in terms of the tube geometry (length, diameter, tube wall thickness), structure (anatase, anatase/rutile) need to be carried out.

The voltage dependence of the photocurrents recorded for annealed nanotubular and compact TiO_2 layers showed essentially an expected Gärtner behavior [98]. For alloyed

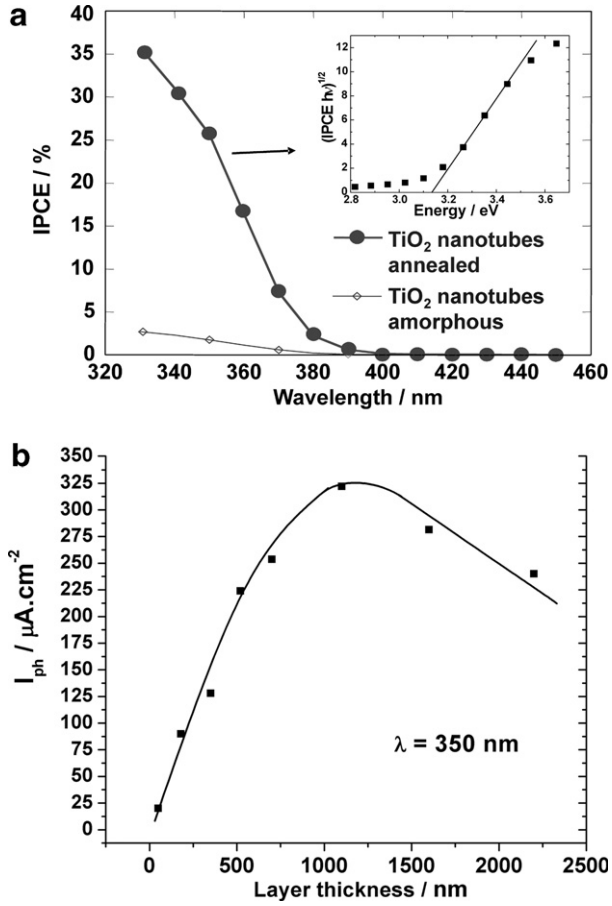

Fig. 10. (a) Photocurrent spectra recorded for as-formed and annealed (450 °C) TiO_2 nanotube layers. An example of the band gap energy (E_g) evaluation is given as an inset; (b) dependence of the photocurrent on the TiO_2 nanotube layer thickness, based on the results from photocurrent transient measured at wavelength of 350 nm.

substrates and the resulting mixed oxides typically the photo-response is significantly lower than for pure TiO_2.

3.2.2. Capacitance measurements

Mott–Schottky type of measurement confirms the assumption that essentially for amorphous nanotubes, only the tube bottoms contribute to an AC response. When annealed, the tube walls contribute correspondingly to their area. The annealed tubes behave as an n-type semiconductor with a doping density of approximately 1.6×10^{20} cm^{-3} [100–102].

3.3. Doping of the tubes

Asahi et al. [105] reported that doping TiO_2 with nitrogen by sputtering in a nitrogen containing gas mixture improves the photoelectrochemical reactivity of TiO_2 films toward organic molecules under visible light illumination. Other doping species such as a number of transition metals [106,107] or non-metals like phosphorus [108], fluorine [109], carbon, [110], sulphur [111], boron [112] have been introduced into TiO_2 compact layers or powders using various techniques. Ion implantation is a most straight-forward approach for doping but, up to now, efforts carried out on TiO_2 (by transition metal implantation) were hampered by the accompanying structural damage [113]. Ion implantation with Cr [114] or thermal treatments to dope C [115,116] have also led to structures with a considerable visible light response. Substantial nitrogen doping of the tube layers was achieved not only by ion implantation [117,118], but also by thermal treatment in NH_3 [99,119].

3.4. Ion intercalation and oxide reduction

Under cathodic polarization a range of valve metal oxides show significant cation in-diffusion, combined with reduction of the oxide. This process is accompanied by alterations in the electronic structure of the oxide (e.g., incorporation of additional states within the band gap that change conductivity and optical properties of the material). The process can generally be ascribed as:

$$M^{IV}O_2 + H^+(Li^+, Na^+) \rightarrow M^{III}O_2H\ (Li^+, Na^+) \qquad (4)$$

This reduction step can be followed by CV curves, as shown in Fig. 11. For many oxides and applied conditions this process is electrochemically reversible [103]. Such intercalating ion uptake and release is applied for example in rechargeable batteries and switchable electrochromic devices.

The cyclic voltammograms in Fig. 11 show curves recorded for the as-formed amorphous and the annealed TiO_2 nanotube layer. The cathodic peak can be ascribed to Ti^{4+} reduction combined with H^+ intercalation, while the anodic peak can be ascribed to the counter reaction (i.e. the H^+ release reaction) [120,121]. The reaction occurs relatively sluggishly (and hardly at all) on the as-formed nanotubular TiO_2 structure, while it is very clearly apparent for the annealed (anatase) structure. The reduction is accompanied with significant alterations in the

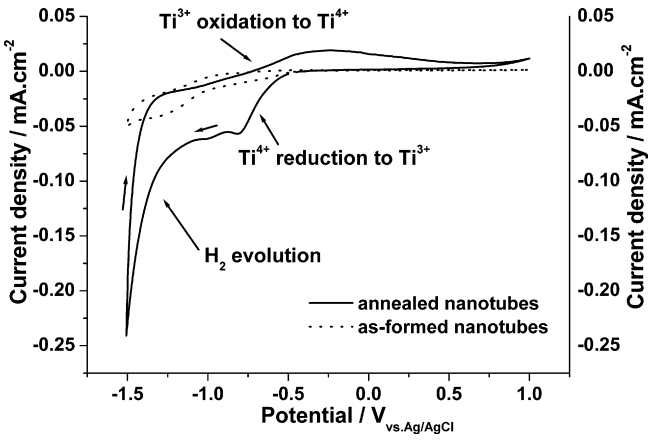

Fig. 11. Cyclic voltammograms recorded for the as-formed and annealed nanotube layers in 1 M $(NH_4)_2SO_4$ showing reduction of Ti^{4+} to Ti^{3+}. At lower potentials, H_2 evolution reaction takes place.

conductivity of the TiO_2 nanotubes from ~15 μS cm^{-1} to ~0.1 μS cm^{-1} [122].

In aqueous electrolytes, up to very alkaline pH values, the most likely mobile intercalation species are protons. Already Dyer and Leach [123] examined oxidized titanium and niobium and found that in aqueous electrolyte hydrogen enters the film under cathodic bias and up to 85% of the material can be converted to TiOOH.

3.5. Reactivity of the tubes

Recently, it has been reported that the nanotube layers have an unusually high reactivity [124,125], i.e. the TiO_2 nanotube system intrinsically is active toward oxygen adsorption [124] – a feature not observed on other, pure anatase or rutile material. This opens up possibilities for fascinating applications since adsorption of oxygen is a prerequisite for a large variety of surface reactions. Furthermore, a clear structure–activity relationship has been observed. Other studies also address adsorption kinetics of alkanes on TiO_2 nanotube arrays and corresponding structure–activity relationships [125].

4. Applications

Particular advantages of regular tube arrays as shown in Fig. 2 are the large surface area and the defined geometry. The defined geometry results in a narrow distribution of diffusion paths not only for entering the tubular depth (e.g., reactants to be transported to the tube bottom) but also for species to be transported through the tube wall, e.g., electrons, holes, ions. Therefore, the system response of ordered tube arrays in applications such as sensing or photocatalysis is expected to be much more defined than using classical high surface area layers – for examples layers where nanoparticles are compacted or sintered to produce an open porous network.

Certain TiO_2 applications require specific crystallographic structures for an optimized performance. For example, the anatase form of TiO_2 shows the highest solar energy conversion efficiency [126,127] and has also the highest activity for catalysis [128,129]. A main challenge regarding the exploitation of TiO_2 in photochemical applications is the large band gap of TiO_2 making photo-induced reactions only possible at excitation <400 nm. Therefore, a main thrust of contemporary research targets the activation of the material for visible (and thus solar) light as schematically shown in Fig. 12a. Two key approaches to achieve this are dye-sensitization [126,127] and so-called doping with species that essentially reduce the band gap of the material [105].

4.1. Solar cells

One of the most promising applications of TiO_2 today is in dye-sensitized solar cells – a concept introduced to a large extent by Grätzel and co-workers [126,127]. The classical Grätzel cell operates with sintered or compressed nanoparticulate TiO_2 layers as electron harvesting material. As such, several microns thick agglomerate layer contains a high number of grain boundaries that can act as recombination sites. It may be expected that optimized nanotube layers can significantly enhance the solar energy conversion efficiency. Dye-sensitization of a TiO_2 electrode with suitable species relies on the fact that certain organic dyes (mainly Ru-complexes) can be anchored on TiO_2 and can inject excited electrons from their LUMO into the conduction band of TiO_2 upon light excitation (for these dyes the LUMO overlaps with the conduction band edge of TiO_2). As the HOMO/LUMO distance of these dyes typically is only 1–2 eV, the reaction can be triggered by visible light. The oxidized dye (that has donated the electron to the TiO_2) can be reduced and thus to be regenerated by a suitable redox species to again form the active (reduced) state on the surface [127]. Also with the nanotube layers successful dye-sensitization has been demonstrated using a commercial Ru-dye [130] and several prototype solar cells have been explored [131–133]. An evaluation of the photocurrent for dye-sensitized TiO_2 nanotube layers is shown in Fig. 12b [134]. It is evident that an optimized tube length for dye-sensitized solar cells seems to be in the range of 20–30 μm.

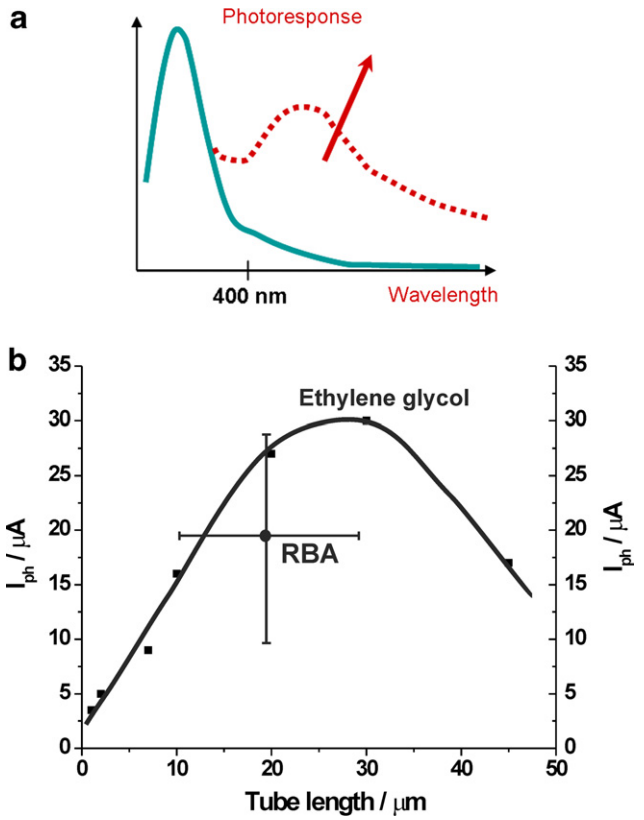

Fig. 12. (a) Schematic representation of activating TiO_2 structures for visible light; (b) photocurrent evaluation of the dye-sensitized nanotube layers grown to different tube length, based on the photocurrent transients at 650 nm [134]. Included are results obtained for RBA TiO_2 nanotubes (as the tubes grow in bundles, the length shows considerable scatter).

It is interesting to note that comparably high conversion efficiencies can also be reached using RBA tubes [133].

4.2. Photocatalysis

After Fujishima and Honda reported for the first time on light-induced water splitting on TiO_2 surfaces the material has been intensively investigated for applications in heterogenous catalysis [135]. Since then, TiO_2 has shown to be an excellent photocatalyst [128,129,136] with a long-term stability, low-cost preparation and a strong enough oxidizing power to be useful for the decomposition of unwanted organic compounds [137–139].

The principle of the photocatalytic decomposition is outlined in Fig. 13a. Photons from a light source excite electrons from the valence band to the conduction band of the TiO_2 – thus charge carrier pairs (consisting of a hole h^+ and an electron e^-) are formed. These charge carriers can migrate to its surface, where they can react with adsorbed molecules. In aqueous solutions valence band holes from TiO_2 typically form $^{\bullet}OH$ radicals, while electrons in the conduction band mainly reduce dissolved molecular oxygen to super-oxide O_2^- anions. These species (in particular $^{\bullet}OH$ radicals) possess such a high oxidation power (redox potential) that they can oxidize essentially all organic molecules present in the solution into carbon dioxide and water [140]. In order to achieve maximal decomposition efficiency, in addition to adequate band edge positions, rapid charge separation and high quantum yield, a large area of the catalyst is desired.

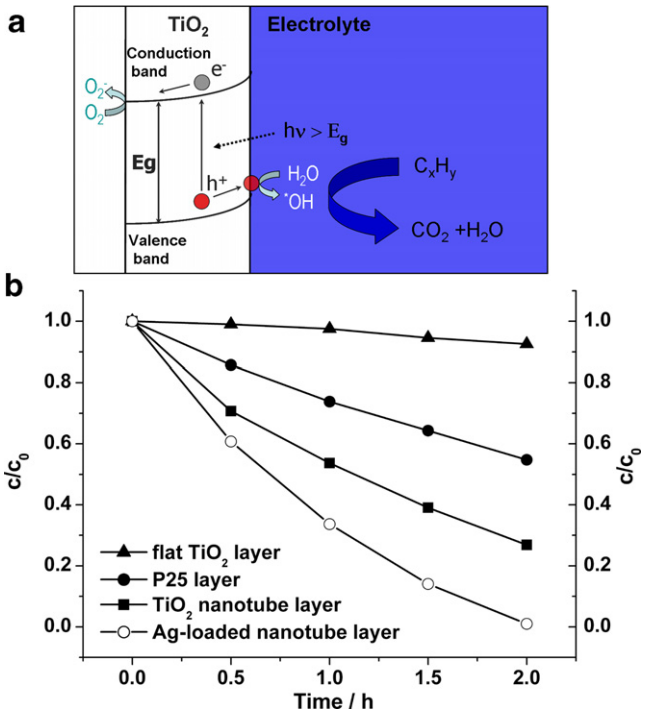

Fig. 13. (a) Principle of the photocatalytic decomposition on the TiO_2 nanoparticle surface; (b) decomposition rates of Acid Orange 7 on different UV-illuminated TiO_2 surfaces.

Photocatalytic activity of TiO_2 nanotubes has been studied by several groups [100,141–144]. Recently it has been demonstrated that the annealed TiO_2 nanotubes show considerably higher decomposition efficiency than a compacted Degussa P25 layer (20–30 nm diameter nanopowder composed of anatase and rutile) under comparable conditions [141], see Fig. 13b.

This efficiency can be even further accelerated by decorating the surface with suitable metallic nanoparticles [144]. Even wider applications for nanotubular TiO_2 layers are provided by the fact that the efficient flow-through photocatalytic membranes could be fabricated that are free-standing and both-side open [88].

4.3. Insertion host and electro-chromic effects

As mentioned above, a specific property of TiO_2 and some other valve metal oxides is its ability to serve as a host for hydrogen ion or lithium ion insertion [103,145–148]. The kinetics and magnitude of ion insertion and the electrochromic reaction (contrast) strongly depend on the ion diffusion length and therefore on geometry of the electrode surface. Due to the specific geometry of the TiO_2 nanotubes, a very high contrast can be obtained using vertically oriented nanotubes [149]. This is shown in Fig. 14, where the electrochromic behavior of a compact TiO_2 layer and a nanotube TiO_2 layer are compared during forward and reverse switching (compare also Fig. 11). For the nanotubes, a strong change of the colour can be observed for the nanotube layer by the naked eye – the colour changes from a very light gray to a solid non-transparent black. On the compact oxide surface, however, hardly any colour change can be observed by eye. Similar findings were

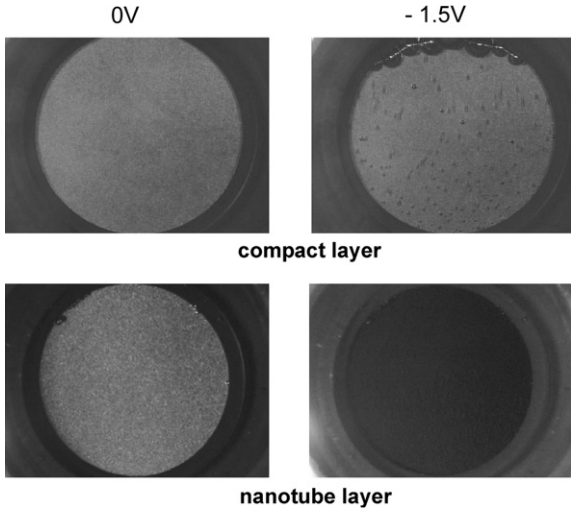

Fig. 14. Optical images showing strong electro-chromic contrast of the nanotube layer at biased states (the voltage values given correspond to the reduced Ti^{III+} (−1.5 V) and oxidized Ti^{IV+} states (0 V). The darkening of the nanotube layers at −1.5 V is due to additional (small band gap) states caused by Ti^{III+} generation resulting in strong alteration of the light absorbance behavior. For comparison, a compact oxide layer is shown resulting in only very weak contrast.

observed for Li insertion reactions [34,150]. The ion intercalation ability can significantly be improved for tubes grown on TiNb [151].

4.4. Adjustable super-wetting properties

For many applications of Ti, alterations of surface topography and wetting behavior are of great importance (e.g. for its biomedical applications). Several approaches using UV light [152,153] or organic monolayers [154] have been reported to control the surface wettability of TiO_2 structures and nanoparticles.

TiO_2 nanotube structures show typically a super-hydrophilic behavior, that is, complete spreading of water on the entire surface and into the tubes. In order to alter the surface properties, octadecylsilane or octadecylphosphonic acid molecules, respectively, can be attached to the TiO_2 nanotube surface [155,156]. The originally completely hydrophilic surface becomes super-hydrophobic with a water contact angle of about $165 \pm 2°$ for the silane-SAMs, and $167 \pm 2°$ for phosphonic acid-SAMs. For comparison, a compact TiO_2 layer shows a contact angle of $107 \pm 2°$ by organic modification.

Using UV illumination the wetting behavior of the SAM-coated tube surface can be altered. After about 12 min for the silane-SAM and 5 min for the phosphonic acid-SAM, the nanotube surface can be changed from super-hydrophobic (~165°) to complete hydrophilic (~0°) contact angles. In fact, the contact angle can be adjusted by the UV exposure time to almost any desired value. XPS studies revealed, in line with literature [154], that during UV light treatment organic monolayers start to decompose by chain scission at the functional end of the C-chain leaving hydrophilic –Si–O^-, –P–O^- groups attached remnant on the TiO_2 surface.

4.5. Biomedical applications

Titanium and its alloys such as Ti–6Al–4V and Ti–6Al–7Nb are widely used in bio-medical applications for orthopaedic, or dental implants due to their good mechanical properties and biochemical compatibility [157]. Therefore, studies on the interaction of the nanotube material in regard to a biorelevant environment are of a very high significance. Mainly two directions have so far been explored with TiO_2 nanotube-coated substrates: (a) hydroxyapatite growth, and (b) cell interactions.

4.5.1. Hydroxyapatite growth

Apatite formation is considered to be essential for the bone-binding ability of biomaterials. In order to improve bioactivity of titanium and to enhance biocompatibility, surface treatments such as hydroxyapatite coating or chemical treatments have been exploited [158–160]. In particular, chemical treatments in NaOH have been examined [160]. An electrochemical method to increase biocompatibility of titanium surfaces is spark anodization [161–164], which typically leads to a formation of a rough random porous TiO_2 layers.

Recently, hydroxyapatite formation on TiO_2 nanotube layers with different tube lengths was investigated [165–167]. The nanotube layers could strongly enhance apatite formation compared with compact TiO_2 layers. Surprisingly, the apatite coverage of the nanotube layers was dependent on the nanotube length – this was attributed to a different surface roughness of the different length nanotubes influencing nucleation of hydroxyapatite precipitation. Annealing the nanotube layers (from amorphous structure) to anatase, or anatase and rutile, further enhanced apatite formation. The induction time for apatite formation on TiO_2 nanotube layers becomes comparable to that for best other treatments of Ti surfaces. In this context, it should be noted that also on commercial biomedical alloys such as Ti6Al4V, Ti6Al7Nb, or experimental biomedical alloys, such as Ti29Nb13Ta4.6Zr (Niinomi alloy), the formation of an ordered and robust oxide nanotube layer is possible [74–76].

4.5.2. Cell response to nanotube layers

Recently, studies on cell interactions with TiO_2 nanotubes show that cell adhesion, proliferation and migration are significantly affected by the nanotube size [168]. Clearly, geometries with a spacing of approximately 15 nm were most stimulating for cell growth and differentiation, whereas diameters of approx. 100 nm lead to a drastically increased cell apoptosis (see Fig. 15). This drastic effect of the nanoscale microenvironment on cell fate was ascribed to specific interactions between a specific nanotube size with the focal adhesion (FA) complex.

4.6. Other aspects

Other applications of the tubes target hydrogen sensing. For instance, Grimes et al. have shown manifold increase in electrical conductivity of the TiO_2 nanotube layer upon exposure to H_2 environments [169]. For example, response in order of several magnitudes has been determined for 1000 ppm H_2 containing nitrogen atmospheres.

Another application of the nanotubes that relies mainly on the large surface area is photochromic switching [170]. By deposition of Ag nanoparticles on the TiO_2 nanotubes, a material can be created that shows considerable photochromic contrast [171]. In general, systems that are based on the deposition of a variety of metallic nanoparticles on TiO_2 can exploit either specific strong support interaction in catalysis, or the material can be dispersed more homogeneously on a substrate. Such effects have been exploited for Pt/Ru-loaded TiO_2 nanotube systems [172], or for Au-loaded nanotubes that show remarkable oxygen sensing capabilities [173].

For many applications thin nanotubular layers of TiO_2 films on a foreign substrate are desired such as on Si-wafer, or on conductive glass (ITO). Several groups reported successful fabrication of oxide nanotube layers from sputter

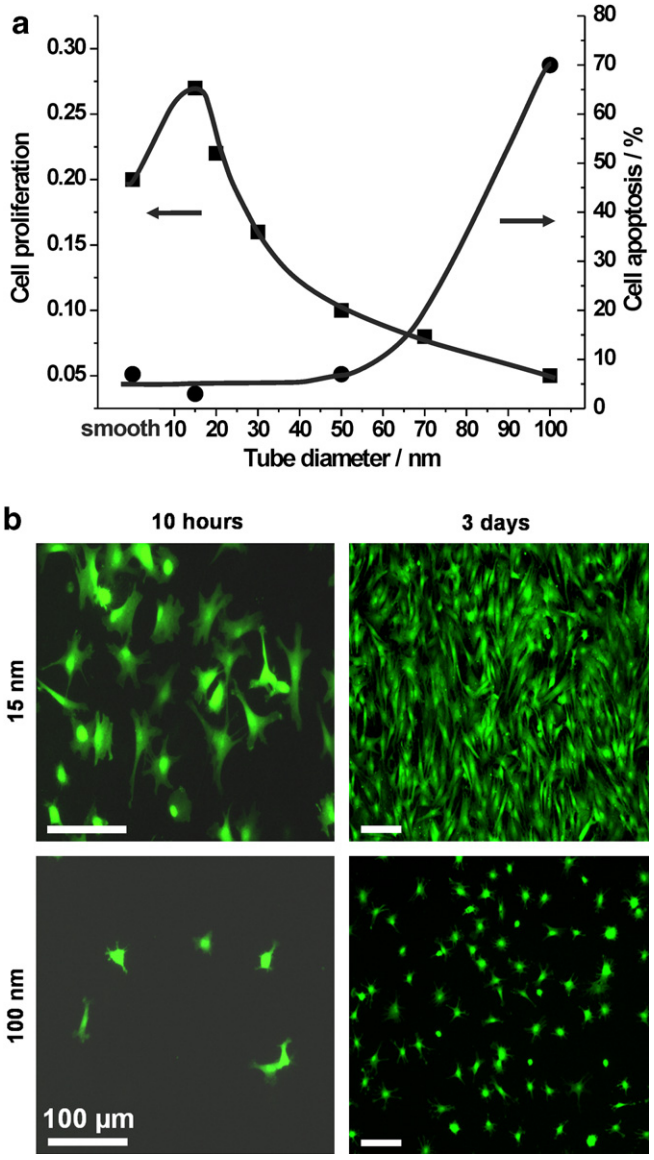

Fig. 15. (a) Proliferation and apoptosis (after 2 days) of cells dispersed on different diameter TiO_2 nanotube layers. Tests done at 37 °C with mesenchymal stem cell (GFP-labeled) using a cell density of 5000 cells/cm^2 and 5 % CO_2; (b) optical images of the cell population on nanotubular TiO_2 surfaces indicating the cell-stimulating effect of a 15 nm diameter nanotube layer compared to a 100 nm diameter [168].

deposited thin titanium films [174–176]. Key is to alter the dissolution rate as much as possible, i.e. to achieve high current efficiency (e.g., by lowering the electrolyte temperature).

The applications of TiO_2 nanotubes can significantly be expanded, if secondary material can successfully be deposited into the tubes. Recently, such an approach has been reported that leads to selective electrodeposition of Cu into the tubes [122], leading to completely filled tubular layers. This is an important step towards magnetic nanotube materials, solid junction solar cells, or biomedical release systems.

The TiO_2 nanotube layers can also be converted to other functional materials [177–180], such as Ba- and Sr-titanates, by an adequate hydrothermal treatment after their formation [177–179].

Acknowledgements

The authors would like to acknowledge financial support from DFG, European Union (6th framework), Socrates Erasmus (Czech Republic), Capes (Brazil), Japanese Ministry of Education, Culture, Sports, Science and Technology (Japan). We also thank R. Beranek, L.V. Taveira, S. Albu, S. Aldabergerova, J. Kunze, I. Sieber, X. Feng, Q. Chen, D. Kim, I. Paramasivam, M. Hueppe, E. Balaur, S. Berger and S. Virtanen for their contributions to this work. Technical assistance of Hans Rollig, Helga Hildebrand, Anja Friedrich, Ullrike Marten-Jahns, Ingeborg Tontsch, Martin Kolacyak and Karl Werner is greatly appreciated. Colleagues from ICT Prague (Dr. J. Krýsa, M. Zlámal) are acknowledged for their help with photocatalytical experiments.

References

[1] Iijima S. Nature 1991;354:56.
[2] Hoyer P. Adv Mater 1996;8:857.
[3] Kasuga T, Hiramatsu M, Hoson A, Sekino T, Niihara K. Langmuir 1998;14:3160.
[4] Krumeich F, Muhr HJ, Niedeberger M, Brieri F, Schnyder B, Nesper R. J Am Chem Soc 1999;121:8324.
[5] Keller F, Hunter MS, Robinson DL. J Electrochem Soc 1953;100:411.
[6] Digg1e JW, Downie TC, Coulding CW. Chem Review 1969;69:365.
[7] O' Sullivan JP, Wood GC. Proc Roy Soc Lon Ser A – Math Phys Sci 1970;317:511.
[8] Thompson G, Wood GC. Anodic films on aluminum. Treatise on materials science and technology, vol. 23. New York: Academic Press; 1983.
[9] Masuda H, Fukuda K. Science 1995;268:1466.
[10] Jessensky O, Muller F, Gösele U. Appl Phys Lett 1998;72:1173.
[11] Ono S, Saito M, Asoh H. Electrochim Acta 2005;51:827.
[12] Chu SZ, Wada K, Inoue S, Isogai M, Yasumori A. Adv Mater 2005;17:2115.
[13] Lee W, Ji R, Gösele U, Nielsch K. Nat Mater 2006;5:741.
[14] Masuda H, Yada K, Osaka A. Jap J Appl Phys 1999;38:L1403.
[15] Al Mawiawi D, Coombs N, Moskovits M. J Appl Phys 1991;70.
[16] Martin CR. Science 1994;266:1961.
[17] Steinhart M, Wendorff JH, Greiner A, Wehrspohn RB, Nielsch K, Schilling J, et al. Science 2002;296:1997.
[18] Zwilling V, Darque-Ceretti E, Boutry-Forveille A, David D, Perrin MY, Aucouturier M. Surf Interface Anal 1999;27:629.
[19] Gong D, Grimes CA, Varghese OK, Chen Z, Dickey EC. J Mater Res 2001;16:3331.
[20] Beranek R, Hildebrand H, Schmuki P. Electrochem Solid-State Lett 2003;6:B12.
[21] Macak JM, Sirotna K, Schmuki P. Electrochim Acta 2005;50:3679.
[22] Macak JM, Tsuchiya H, Schmuki P. Angew Chem 2005;44:2100.
[23] Taveira LV, Macak JM, Tsuchiya H, Dick LFP, Schmuki P. J Electrochem Soc 2005;152:B405.
[24] Ghicov A, Tsuchiya H, Macak JM, Schmuki P. Electrochem Commun 2005;7:505.
[25] Macak JM, Tsuchiya H, Taveira L, Aldabergerova S, Schmuki P. Angew Chem Int Ed 2005;44:7463.
[26] Tsuchiya H, Macak JM, Taveira L, Balaur E, Ghicov A, Sirotna K, et al. Electrochem Commun 2005;7:576.

[27] Taveira LV, Macak JM, Sirotna K, Dick LFP, Schmuki P. J Electrochem Soc 2005;153:B137.
[28] Macak JM, Schmuki P. Electrochim Acta 2006;52:1258.
[29] Albu SP, Ghicov A, Macak JM, Schmuki P. Phys Stat Sol (RRL) 2007;1:R65.
[30] Schmuki P, Macak JM, Tsuchiya H. In: Schmuki P, Lockwood DJ, Isaacs HS, Ogata Y, Seo M, editors. Proceedings of the symposium "Pits and pores: formation, properties and significance for advanced materials". PV of ECS Hawaii meeting 2004. The Electrochemical Society.
[31] Bauer S, Kleber S, Schmuki P. Electrochem Commun 2006;8:1321.
[32] Kunze J, Ghicov A, Hildebrand H, Macak JM, Taveira L, Schmuki P. Z Phys Chem 2006;129:1561.
[33] Yasuda K, Macak JM, Berger S, Ghicov A, Schmuki P. J Electrochem Soc 2007;154:C472.
[34] Lee W-J, Alhoshan M, Smyrl WH. J Electrochem Soc 2006;153:B499.
[35] Raja KS, Misra M, Paramguru K. Electrochim Acta 2005;51:154.
[36] Zhao J, Wang X, Chen R, Li L. Solid State Commun 2005;134:705.
[37] Bayoumi FM, Ateya BG. Electrochem Commun 2005;8:38.
[38] Li H, Bai X, Ling Y, Li J, Zhang D, Wang J. Electrochem Solid-State Lett 2006;9:B28.
[39] Sklar GP, Singhm H, Mahajan V, Gorhe D, Namjoshi SA, La Combe JC. Mater Res Soc Symp Proc 2005;876E:R1.2.
[40] Xin Y, Jin Z, Hou F, Wang Y. J Am Ceram Soc 2007;90:2384.
[41] Kaneco S, Chen Y, Westerhoff P, Crittenden JC. Scripta Mater 2007;56:373.
[42] Regonini D, Bowen CR, Stevens R, Allsopp D, Jaroenworaluck A. Phys Stat Sol (A) 2007;204:1814.
[43] Bestetti M, Franz S, Cuzzolin M, Arosio P, Cavallotti PL. Thin Solid Films 2007;515:5253.
[44] Tsuchiya H, Schmuki P. Electrochem Commun 2004;6:1131.
[45] Tsuchiya H, Macak JM, Sieber I, Schmuki P. Small 2005;1:722.
[46] Tsuchiya H, Macak JM, Taveira LV, Ghicov A, Schmuki P. Corros Sci 2005;43:3324.
[47] Lee WJ, Smyrl WH. Electrochem Solid-State Lett 2005;8:B7.
[48] Sieber I, Hildebrand H, Friedrich A, Schmuki P. Electrochem Commun 2005;7:97.
[49] Ono S, Nagasaka T, Shimazaki H, Asoh H. In: Schmuki P, Lockwood DJ, Ogata YH, Isaacs HS, editors. Pits and pores II: Formation properties and significance for advanced materials, PV 2004-19. The Electrochemical Society Proceedings Series. Pennington, NJ. p. 123.
[50] Choi J, Lim JH, Lee SCh, Chang JH, Kim KJ, Cho MA. Electrochim Acta 2006;51:5502.
[51] Choi J, Lim JH, Lee J, Kim KJ. Nanotechnology 2007;18:055603.
[52] Karlinsey R. Electrochem Commun 2005;7:1190.
[53] Tsuchiya H, Macak JM, Sieber I, Taveira L, Ghicov A, Sirotna K, et al. Electrochem Commun 2005;7:295.
[54] de Tacconi NR, Chenthamarakshan CR, Yogeeswaran G, Watcharenwong A, de Zoysa RS, Basit NA, et al. J Phys Chem B 2006;110:25347.
[55] Berger S, Tsuchiya H, Ghicov A, Schmuki P. Appl Phys Lett 2006;88:203119.
[56] Sieber I, Schmuki P. J Electrochem Soc 2005;152:C639.
[57] Sieber I, Kannan B, Schmuki P. Electrochem Solid-State Lett 2005;8:J10.
[58] El-Sayed H, Singh S, Greiner MT, Kruse P. Nano Lett 2006;6:2995.
[59] Tsuchiya H, Schmuki P. Electrochem Commun 2005;7:49.
[60] Young L. Anodic oxide films. New York: Plenum; 1961.
[61] Vermilyea DA. Anodic films. In: Advances in electrochemistry and electrochemical engineering. London: Wiley; 1963. p. 248.
[62] Schultze JW, Lohrengel MM. Electrochim Acta 2000;45:2499.
[63] Marchenoir JC, Loup JP, Masson J. Thin Solid Films 1980;66:357.
[64] Arsov L, Froehlicher M, Froment M, Hugot-le-Goff A. J Chim Phys 1975;3:275.
[65] Schultze JW, Lohrengel MM, Ross D. Electrochim Acta 1983;28:973.
[66] Yahalom J, Zahavi J. Electrochim Acta 1970;15:1429.
[67] Marchenoir J-C, Gautron J, Loup JP. Metaux Corrosion-industrie 1977:83.
[68] Delplancke J-L, Winand R. Electrochim Acta 1988;33:1551.
[69] Macak JM, Albu SP, Schmuki P. Phys Stat Sol (RRL) 2007;1:R181.
[70] Tsuchiya H, Berger S, Macak JM, Ghicov A, Schmuki P. Electrochem Commun 2007;9:2397.
[71] Ghicov A, Aldabergerova S, Tsuchiya H, Schmuki P. Angew Chem Int Ed 2006;45:6993.
[72] Yasuda K, Schmuki P. Adv Mater 2007;19:1757.
[73] Yasuda K, Schmuki P. Electrochim Acta 2007;52:4053.
[74] Macak JM, Tsuchiya H, Taveira L, Ghicov A, Schmuki P. J Biomed Mat Res 2005;75A:928.
[75] Tsuchiya H, Macak JM, Ghicov A, Schmuki P. Small 2006;2:888.
[76] Tsuchiya H, Macak JM, Ghicov A, Tang YC, Fujimoto S, Niinomi M, et al. Electrochim Acta 2006;52:94.
[77] Kuroda D, Niinomi M, Morinaga M, Kato Y, Yashiro T. Mater Sci Eng A 1998;243:244.
[78] Feng X, Macak JM, Albu SP, Schmuki P. Acta Biomater, in press.
[79] Feng X, Macak JM, Schmuki P. Electrochem Commun 2007;9:2403.
[80] Tsuchiya H, Berger S, Macak JM, Munoz AG, Schmuki P. Electrochem Commun 2007;9:545.
[81] Nakayama K et al. In: 208th ECS Meeting 2005, Abstract Nos. 819 and 843.
[82] Hahn R, Macak JM, Schmuki P. Electrochem Commun 2007;9:947.
[83] Richter Ch, Wu Z, Panaitescu E, Willey RJ, Menon L. Adv Mater 2007;19:946.
[84] Parkhutik VP, Shershulsky VI. J Phys D 1992;25:1258.
[85] Yasuda K, Schmuki P. Electrochem Commun 2007;9:615.
[86] Macak JM, Hildebrand H, Marten-Jahns U. J Electroanal Chem, submitted for publication.
[87] Macak JM, Albu SP, Kim DH, Paramasivam I, Aldabergerova S, Schmuki P. Electrochem Solid-State Lett 2007;10:K28.
[88] Albu SP, Ghicov A, Macak JM, Hahn R, Schmuki P. Nano Lett 2007;7:1286.
[89] Varghese OK, Gong D, Paulose M, Grimes CA, Dickey EC. J Mater Res 2003;18:156.
[90] Ghicov A, Tsuchiya H, Macak JM, Schmuki P. Phys Stat Sol A 2006;203:R28.
[91] Macak JM, Aldabergerova S, Ghicov A, Schmuki P. Phys Stat Sol A 2006;203:R67.
[92] Zhao J, Wang X, Sun T, Li L. Nanotechnology 2005;16:2450.
[93] Albu SP, submitted for publication.
[94] Arbiol J, Cerda J, Dezanneau G, Cicera A, Peiro F, Cornet A, et al. J Appl Phys 2002;92:853.
[95] Tryba B, Moravski AW, Inagaki M. Appl Catal B: Environ 2003;52:203.
[96] Shimizu K, Kobayashi K. J Surf Finish Soc Jpn 1995;46:402.
[97] Lausmaa J. J Electron Spectrosc Relat Phenom 1996;81:343.
[98] Beranek R, Tsuchiya H, Sugishima T, Macak JM, Taveira L, Fujimoto S, et al. Appl Phys Lett 2005;87:243114.
[99] Macak JM, Ghicov A, Hahn R, Tsuchiya H, Schmuki P. J Mater Res 2006;21:2824.
[100] Xie Y. Adv Func Mater 2006;16:1823.
[101] Tsuchiya H, Macak JM, Ghicov A, Räder A, Taveira LV, Schmuki P. Corr Sci 2007;49:203.
[102] Taveira LV, Macak JM, Schmuki P, Sagues A. J Electrochem Soc, submitted for publication.
[103] Kavan L, Grätzel M, Gilbert SE, Klemenz C, Scheel HJ. J Am Chem Soc 1996;118:6716.
[104] Macak JM, submitted for publication.
[105] Asahi R, Morikawa T, Ohwaki T, Aoki A, Taga Y. Science 2001;293:269.
[106] Wilke K, Breuer HD. J Photochem Photobiol A 1999;127:107.
[107] Lin L, Lin W, Zhu Y, Zhao B, Xie Y. Chem Lett 2005;34:284.
[108] Anpo M. Catal Surv Jpn 1997;1:169.

[109] Yamaki T, Umebayashi T, Sumita T, Yamamoto S, Maekawa M, Kawasuso A, et al. Nucl Instrum Methods Phys Res Sec B 2003;206:254.
[110] Sakthivel S, Kisch H. Angew Chem Int Ed 2003;42:4908.
[111] Ohno T, Mitsui T, Matsumura M. Chem Lett 2003;32:364.
[112] Zhao W, Ma W, Chen C, Zhao J, Shuai Z. J Am Chem Soc 2004;126:4782.
[113] Tsuji H, Sugahara H, Gotoh Y, Ishikawa J. Nucl Instr Meth Phys Res B 2003;206:249.
[114] Ghicov A, Schmidt B, Kunze J, Schmuki P. Chem Phys Lett 2007;433:323.
[115] Park JH, Kim S, Bard AJ. Nano Lett 2006;6:24.
[116] Hahn R, Ghicov A, Salonen J, Schmuki P. Nanotechnology 2007;18:105604.
[117] Ghicov A, Macak JM, Tsuchiya H, Kunze J, Heaublein V, Frey L, et al. Nano Lett 2006;6:1080.
[118] Ghicov A, Macak JM, Tsuchiya H, Kunze J, Haeublein V, Kleber S, et al. Chem Phys Lett 2005;419:426.
[119] Vitiello RP, Macak JM, Ghicov A, Tsuchiya H, Dick LFP, Schmuki P. Electrochem Commun 2006;8:544.
[120] Sakai N, Fujishima A, Watanabe T, Hashimoto K. J Electrochem Soc 2001;148:E395.
[121] Pelouchova H, Janda P, Weber J, Kavan L. J Electroanal Chem 2004;566:73.
[122] Macak JM, Gong BG, Hueppe M, Schmuki P. Adv Mater. 10.1002/adma.200602549.
[123] Dyer CK, Leach JSL. J Electrochem Soc 1978;125:23.
[124] Funk S, Hokanen B, Burghaus U, Ghicov A, Schmuki P. Nano Lett 2007:1091.
[125] Hokkanen B, Funk S, Burghaus U, Ghicov A, Schmuki P. Surf Sci 2007;601:4620.
[126] O'Regan B, Grätzel M. Nature 1991;353:737.
[127] Grätzel M. Nature 2001;414:338.
[128] Linsebigler AL, Lu G, Yates JT. Chem Rev 1995;95:735.
[129] Hofmann MR, Martin ST, Choi W, Bahnemann DW. Chem Rev 1995;95:69.
[130] Macak JM, Tsuchiya H, Ghicov A, Schmuki P. Electrochem Commun 2005;7:1138.
[131] Wang H, Yip CT, Cheng KY, Djurisic AB, Xie MH, Leung YH, et al. Appl Phys Lett 2006;89:023508.
[132] Zhu K, Neale NR, Miedaner A, Frank AJ. Nano Lett 2007;7:69.
[133] Hahn R et al. Phys Stat Sol (RRL) 2007;1:R135.
[134] Ghicov A, submitted for publication.
[135] Fujishima A, Honda K. Nature 1972;238:37.
[136] Mills A, Le Hunte S. J Photochem Photobiol A 1997;108:1.
[137] Kiriakidou F, Kondarides DI, Verykios XE. Catal Today 1999;54:119.
[138] Zhang F, Zhao J, Shen T, Hidaka H, Pelizzetti E, Serpone N. Appl Catal B 1998;15:147.
[139] Krýsa J, Keppert M, Waldner G, Jirkovský J. Electrochim Acta 2005;50:5255.
[140] Ollis DF, Al-Ekabi H. Photocatalytic purification and treatment of water and air. Amsterdam: Elsevier; 1993.
[141] Macak JM, Zlamal M, Krysa J, Schmuki P. Small 2007;3:300.
[142] Lai Y, Sun L, Chen Y, Zhuang H, Lin Ch, Chin JW. J Electrochem Soc 2006;153:D123.
[143] Zhuang H, Lin Ch, Lai Y, Sun L, Li J. Environ Sci Technol 2007;41:4735.
[144] Paramasivam I, submitted for publication.
[145] Philips II, Poole P, Shreir LL. Corros Sci 1972;12:855.
[146] Foroulis ZA. J Electrochem Soc 1981;128:219.
[147] Brauer E, Gruner R, Rauch F. Ber Bunsen Phys Chem 1983;87:341.
[148] Blackwood DJ, Peter LM, Bishop HE, Chalker PR, Williams DE. Electrochim Acta 1989;34:1401.
[149] Ghicov A, Tsuchiya H, Hahn R, Macak JM, Munoz AG, Schmuki P. Electrochem Commun 2006;8:528.
[150] Hahn R, Ghicov A, Tsuchiya H, Macak JM, Munoz AG, Schmuki P. Phys Stat Sol A 2007;204:1281.
[151] Ghicov A, submitted for publication.
[152] Wang R, Hashimoto K, Fujishima A, Chikuni M, Kojima E, Kitamura A, et al. Nature 1997;388:431.
[153] Wang R, Hashimoto K, Fujishima A, Chikuni M, Kojima E, Kitamura A, et al. Adv Mater 1998;10:135.
[154] Lee JP, Kim HK, Park CR, Park G, Kwak HT, Koo SM, Sung MM. J Phys Chem B 2003;107:8997.
[155] Balaur E, Macak JM, Taviera L, Tsuchiya H, Schmuki P. Electrochem Commun 2005;7:1066.
[156] Balaur E, Macak JM, Tsuchiya H, Schmuki P. J Mater Chem 2005;15:4488.
[157] Brunette DM, Tengvall P, Textor M, Thomsen P. Titanium in medicine. Berlin: Springer; 2001.
[158] Roome CM, Adam CD. Biomaterials 1995;16:69.
[159] Weng J, Liu Q, Wolke JGC, Zhang X, de Grood K. Biomaterials 1997;18:1027.
[160] Jonasova L, Müller FA, Helebrant A, Strnad J, Greil P. Biomaterials 2002;23:3095.
[161] Sul YT, Johansson CB, Petronis S, Krozer A, Jeong Y, Wennerberg A, Albrektsson T. Biomaterials 2002;23:491.
[162] Mueller Y, Virtanen S. In: Schmuki P, Lockwood DJ, Ogata YH, Isaacs HS, editors. Pits and pores II. The Electrochemical Society Proceedings Series. PV 2000-25, Pennington, NJ; 2000. p. 294.
[163] Yang B, Uchida M, Kim HM, Zhang X, Kokubo T. Biomaterials 2004;25:1003.
[164] Song WH, Jun YK, Han Y, Hong SH. Biomaterials 2004;25:3341.
[165] Oh SH, Finones RR, Daraio Ch, Chen LH, Jin S. Biomaterials 2005;26:4938.
[166] Tsuchiya H, Macak JM, Muller L, Kunze J, Muller F, Greil SP, et al. J Biomed Mat Res 2006;77A:534.
[167] Raja KS, Misra M, Paramguru K. Mater Lett 2005;59:2137.
[168] Park J, Bauer S, Von der Mark K, Schmuki P. Nano Lett 2007;7:1686.
[169] Varghese OK, Gong D, Paulose M, Ong KG, Dickey EC, Grimes CA. Adv Mater 2003;15:624.
[170] Ohko Y, Tatsuma T, Fuji T, Naoi K, Niwa C, Kubota Y, et al. Nat Mater 2003;2:29.
[171] Paramasivam I, Macak JM, Ghicov A, Schmuki P. Chem Phys Lett 2007;445:223.
[172] Macak JM, Barczuk PJ, Tsuchiya H, Nowakowska MZ, Ghicov A, Chojak M, et al. Electrochem Commun 2005;7:1417.
[173] Macak JM, Schmidt-Stein F, Schmuki P. Electrochem Commun 2007;9:1783.
[174] Macak JM, Tsuchia H, Berger S, Bauer S, Fujimoto S, Schmuki P. Chem Phys Lett 2006;428:421.
[175] Premchand YD, Djenizian T, Vacandio F, Knauth P. Electrochem Commun 2005;8:1840.
[176] Yu X, Li Y, Ge W, Yang Q, Zhu N, Zadeh KK. Nanotechnology 2006;17:808.
[177] Padture NT, Wei X. J Am Ceram Soc 2003;86:2215.
[178] Wei X, Vasiliev AL, Padture NP. J Mater Res 2005;20:2140.
[179] Zhao J, Wang X, Chen R, Li L. Mater Lett 2005;59:2329.
[180] Bavykin DV, Friedrich JM, Walsch FC. Adv Mater 2006;18:1.
[181] Fujishima A, Rao TN, Tryk DA. J Photochem Photobiol C: Photochem Rev 2000;1:1.
[182] Valden M, Lai X, Goodman DW. Science 1998;281:1647.
[183] Lopez N, Janssens TVW, Clausen BS, Xu Y, Mavrikakis M, Bligaard T, et al. J Catal 2004;223:232.
[184] Sberveglieri G, editor. Gas sensors. Dordrecht: Kluwer Academic Publishing; 1992.
[185] Kirner U et al. Sensor Actuat B 1990;1:103.
[186] Kingery WD, Bowen HK, Uhlmann DR. Introduction to ceramics. New York: Wiley; 1976.
[187] Uchino K. Ferroelectric devices. New York: Marcel Dekker; 2000.
[188] Samsonov GV. The oxide handbook. New York: Wiley; 1982.
[189] Sharma AK. Thin Solid Films 1992;208:48.
[190] Garcia-Vergara SJ, Skeldon P, Thompson GE, Habazaki H. Electrochim Acta 2006;52:681.